BIOCHEMISTRY
including biophysical chemistry & molecular biology

Article

pubs.acs.org/biochemistry

Functional Annotation and Three-Dimensional Structure of an Incorrectly Annotated Dihydroorotase from cog3964 in the Amidohydrolase Superfamily

Argentina Ornelas,[†] Magdalena Korczynska,[§] Sugadev Ragumani,[‡] Desigan Kumaran,[‡] Tamari Narindoshvili,[†] Brian K. Shoichet,*[,§] Subramanyam Swaminathan,*[,‡] and Frank M. Raushel*[,†]

[†]Department of Chemistry, P.O. Box 30012, Texas A&M University, College Station, Texas 77842-3012, United States

[‡]Biology Department, Brookhaven National Laboratory, P.O. Box 5000, Upton, New York 11973-5000, United States

[§]Department of Pharmaceutical Chemistry, University of California, San Francisco, 1700 Fourth Street, San Francisco, California 94158-2330, United States

Supporting Information

ABSTRACT: The substrate specificities of two incorrectly annotated enzymes belonging to cog3964 from the amidohydrolase superfamily were determined. This group of enzymes are currently misannotated as either dihydroorotases or adenine deaminases. Atu3266 from *Agrobacterium tumefaciens* C58 and Oant2987 from *Ochrobactrum anthropi* ATCC 49188 were found to catalyze the hydrolysis of acetyl-(*R*)-mandelate and similar esters with values of k_{cat}/K_m that exceed 10^5 M^{-1} s^{-1}. These enzymes do not catalyze the deamination of adenine or the hydrolysis of dihydroorotate. Atu3266 was crystallized and the structure determined to a resolution of 2.62 Å. The protein folds as a distorted $(\beta/\alpha)_8$ barrel and binds two zincs in the active site. The substrate profile was determined via a combination of computational docking to the three-dimensional structure of Atu3266 and screening of a highly focused library of potential substrates. The initial weak hit was the hydrolysis of *N*-acetyl-D-serine (k_{cat}/K_m = 4 M^{-1} s^{-1}). This was followed by the progressive identification of acetyl-(*R*)-glycerate (k_{cat}/K_m = 4 × 10^2 M^{-1} s^{-1}), acetyl glycolate (k_{cat}/K_m = 1.3 × 10^4 M^{-1} s^{-1}), and ultimately acetyl-(*R*)-mandelate (k_{cat}/K_m = 2.8 × 10^5 M^{-1} s^{-1}).

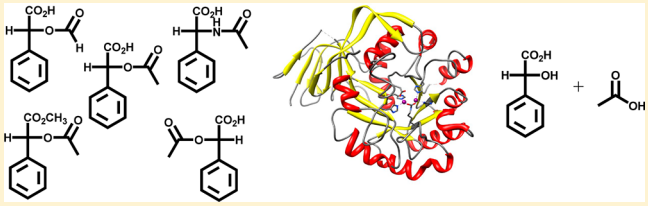

The development of a comprehensive strategy for the functional annotation of proteins and enzymes whose sequences have been deposited in public databases has proven to be a difficult and persistent challenge. Utilization of homology-based sequence comparisons for functional annotation of newly sequenced genes can often lead to the annotation of the wrong function when unreasonable threshold values are used.[1−3] The end result is often a misrepresentation of the potential metabolic transformations contained within a given organism. In addition to the misannotation of enzyme function, there is a significant fraction of the total gene inventory that is simply not annotated.[4−6] This observation suggests that a substantial segment of the metabolic landscape remains to be discovered.

In many cases, functional annotation of newly sequenced genes can be strategically approached by the integration of structural genomics,[7,8] computational docking,[9,10] high-throughput screening,[11] and genome context analysis.[12] We have focused our efforts toward the development of a simple and integrated strategy for functional annotation that is based on an assault on the amidohydrolase superfamily (AHS) of enzymes. This superfamily was first identified and recognized from the three-dimensional structural similarities among urease, adenosine deaminase, and phosphotriesterase.[13] The amidohydrolase superfamily is characterized structurally by an active site that contains a mono- or binuclear metal center embedded at the C-terminal end of a distorted $(\beta/\alpha)_8$ barrel protein fold. Typically identified by an HxH motif after the C-terminal end of β-strand 1, the enzymes from the AHS also contain other coordinating ligands to the metal center at the ends of β-strands 4−6 and 8.[14] The metal center serves in the activation of a hydrolytic water molecule for nucleophilic attack and to stabilize the transition state. Most of the reactions catalyzed by this diverse superfamily involve the hydrolysis of C−O, C−N, or P−O bonds. However, some members of this superfamily also catalyze decarboxylation, hydration, or isomerization reactions.[15−17] Enzymes from the AHS catalyze reactions in the metabolism of carbohydrates, amino acids, and nucleic acids and the degradation of organophosphate esters.

The AHS has been organized into 24 Clusters of Orthologous Groups (COG).[18,19] One of these clusters, cog3964, represents one of the smaller homologous groups of amidohydrolases, with approximately 200 sequences identified to date. A sequence similarity network for this COG is presented in Figure 1 at an *E* value cutoff of 10^{-70}. Some members of cog3964 have been annotated as dihydroorotases,

Received: October 31, 2012
Revised: December 7, 2012
Published: December 10, 2012

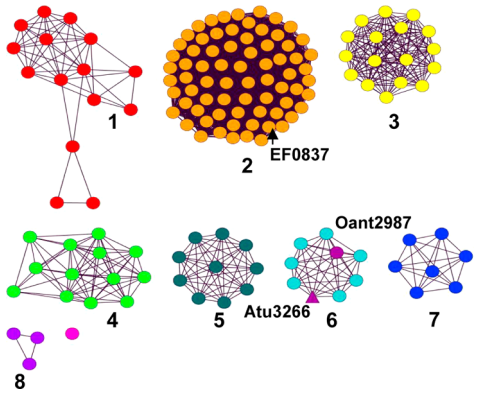

Figure 1. Sequence similarity network for the organization of cog3964 within the amidohydrolase superfamily.[18,19] Each node in the diagram represents a sequence that has been annotated as belonging to cog3964, and each edge represents the pairwise connection between two sequences at a BLAST *E* value of better than 10^{-70}. Atu3266 and Oant2987 are found in group 6 and are colored purple.

which catalyze the interconversion of dihydroorotate and *N*-carbamoyl aspartate,[20,21] while other members have been annotated as catalyzing the deamination of adenine.[22] Experimentally annotated dihydroorotases are found in cog0044 and cog0418. Structurally and experimentally characterized adenine deaminases are found in cog1001[22] and in cog1816.[23] A straightforward comparison of the amino acid sequences found within the proteins from cog3964 with the experimentally annotated adenine deaminases and dihydroorotases clearly indicates that the residues required for substrate recognition of adenine and/or dihydroorotate are not conserved. This observation suggests that either these annotations are clearly wrong for cog3964 or a previously unrecognized novel constellation of amino acids has evolved for the deamination of adenine or the hydrolysis of dihydroorotate.

In this paper, we report the three-dimensional crystal structure and substrate profile for two enzymes from cog3964: Atu3266 from *Agrobacterium tumefaciens* and Oant2987 from *Ochrobactrum anthropi*. Neither of these enzymes is able to catalyze the hydrolysis of dihydroorotate or the deamination of adenine. We have utilized a focused compound library and computational docking to discover that these two enzymes from cog3964 actually catalyze the hydrolysis of acetylated α-hydroxyl carboxylates as shown in Scheme 1. The best substrate identified to date is acetyl-(*R*)-mandelate. This compound is enzymatically hydrolyzed with a k_{cat}/K_m value of 2.8×10^5 M^{-1} s^{-1}.

Scheme 1

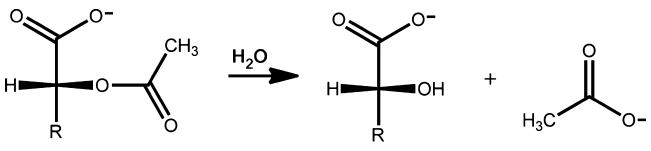

MATERIALS AND METHODS

Materials. The genomic DNA from *O. anthropi* strain ATCC-49188 was purchased from the American Type Culture Collection (ATCC). DNA sequencing reactions were conducted at the Gene Technology Laboratory at Texas A&M University. The chemicals utilized in the expression, purification, and screening of Atu3266 and Oant2987 were obtained from Sigma-Aldrich, unless stated otherwise. The preparation of the acylated compounds tested for substrate activity is provided in the Supporting Information. The structures for many of these compounds are provided in Schemes 2 and 3. The pET-20b(+) expression vector and Rosetta-gami B(DE3)pLysS competent cells were obtained from Novagen. The acetate and formate detection kits were purchased from Megazyme. *N*-Acetyl-DL-phenylglycine was purchased from Chem-Impex International. 3-Bromomandelic acid and 4-bromomandelic acid were purchased from Oakwood Products, Inc.

Gene Cloning. The gene for Oant2987 (gi|153010310) from *O. anthropi* was amplified by polymerase chain reaction using the primer pair of 5′-ACAGGAGCCATATGATTTCCGGTGAACAGGCGAAGCCG-3′ containing an NdeI restriction site and 5′-ACGCGAATTCCCAGCGCCACGAATAGCCATGGCTATGGC-3′ having an EcoRI restriction site. Oant2987 was inserted into a pET-20b(+) vector that had been previously digested with NdeI and EcoRI. The gene for Atu3266 was initially cloned by the New York SGX Research Consortium for Structural Genomics from *A. tumefaciens* (gi|159185666). The poor overexpression and solubility of this clone in BL21(DE3) cells led to the removal of the gene from its original TOPO-isomerase vector, pSGX3(BC), using the restriction sites CCGC↓GG and CA↓TATG of the construct and removing the gene by digestion with SacII and NdeI restriction enzymes. The gene was transferred to a pET-20b(+) vector previously digested with the same restriction enzymes. The modified clone contained a His_6 C-terminal purification tag.

Expression and Purification of Oant2987 and Atu3266. The plasmid containing the gene for Oant2987 was transformed into BL21(DE3) and plated on LB agar/ampicillin plates. A single colony was inoculated into overnight cultures containing 5 mL of LB medium supplemented with 100 μg/mL ampicillin. These cultures were utilized to make 1 L cultures containing the same concentration of ampicillin and grown at 30 °C in a shaker-incubator. After an OD_{600} of 0.3 had been reached, the cells were supplemented with 150 μM 2,2′-bipyridyl to coordinate excess ferric iron from the medium. At an OD_{600} of 0.6, the cells were induced with 200 μM IPTG and the addition of 1.0 mM $Zn(OAc)_2$. The temperature upon induction was reduced to 20 °C, and the cultures were allowed to continue to grow for an additional 12 h. The cells were harvested by centrifugation and frozen at −80 °C. The frozen cell pellet was thawed and resuspended in 60 mL of 50 mM HEPES buffer (pH 7.6) (buffer A). The cells were supplemented with 10 μg/mL phenylmethanesulfonyl fluoride (PMSF) and lysed by sonication at 0 °C. The supernatant solution was treated with 2% (w/v) protamine sulfate and centrifuged. The protein was precipitated with ammonium sulfate between 40 and 80% saturation. The protein pellet was resuspended with a minimal amount of buffer A and loaded onto a Superdex 200 gel filtration column. The fractions of interest were collected and subsequently loaded onto a Resource Q column. The protein was eluted from the column with a gradient of 20 mM HEPES buffer (pH 7.6) containing 1 M NaCl (buffer B). The purity of Oant2987 was greater than 95% based on sodium dodecyl sulfate−polyacrylamide gel electrophoresis (SDS−PAGE).

The plasmid containing the gene for Atu3266 was transformed into Rosetta-gami B(DE3)pLysS electrocompetent

dx.doi.org/10.1021/bi301483z | *Biochemistry* 2013, 52, 228−238

Scheme 2

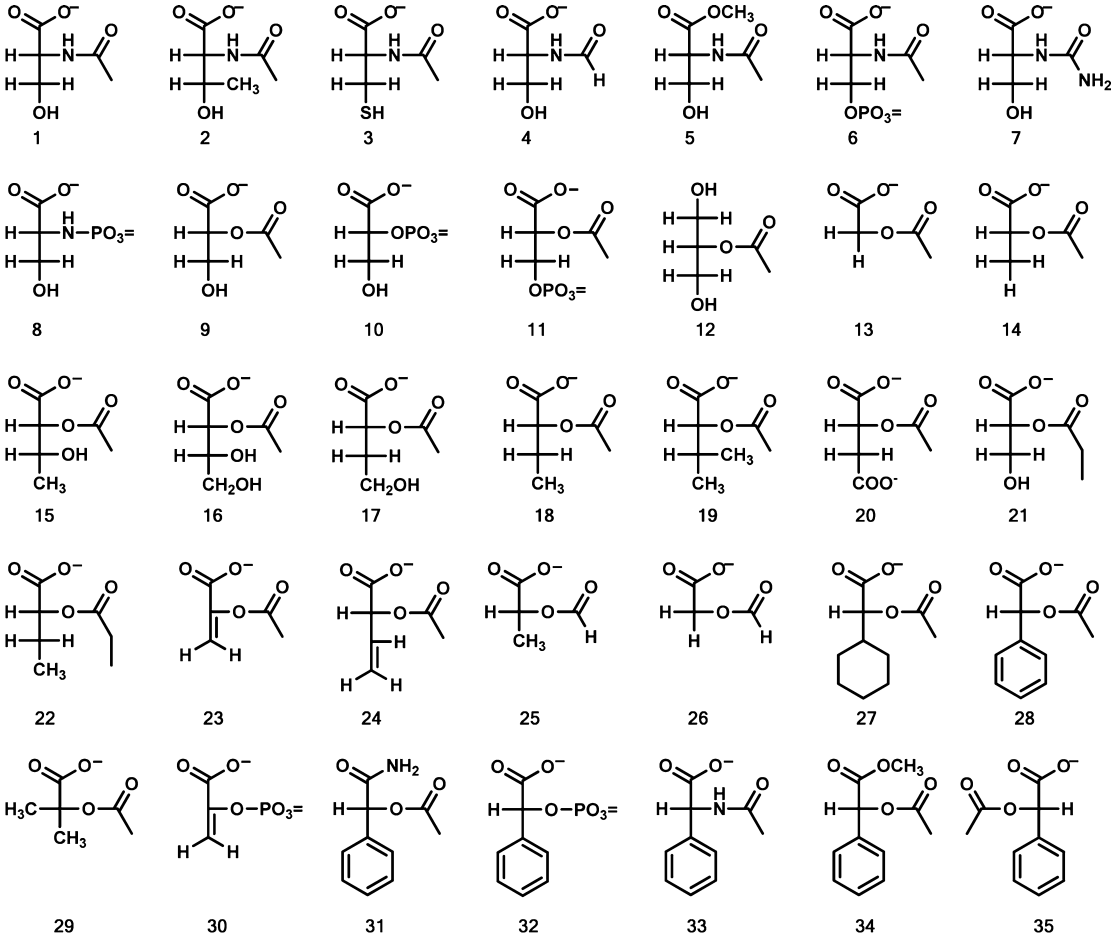

Scheme 3

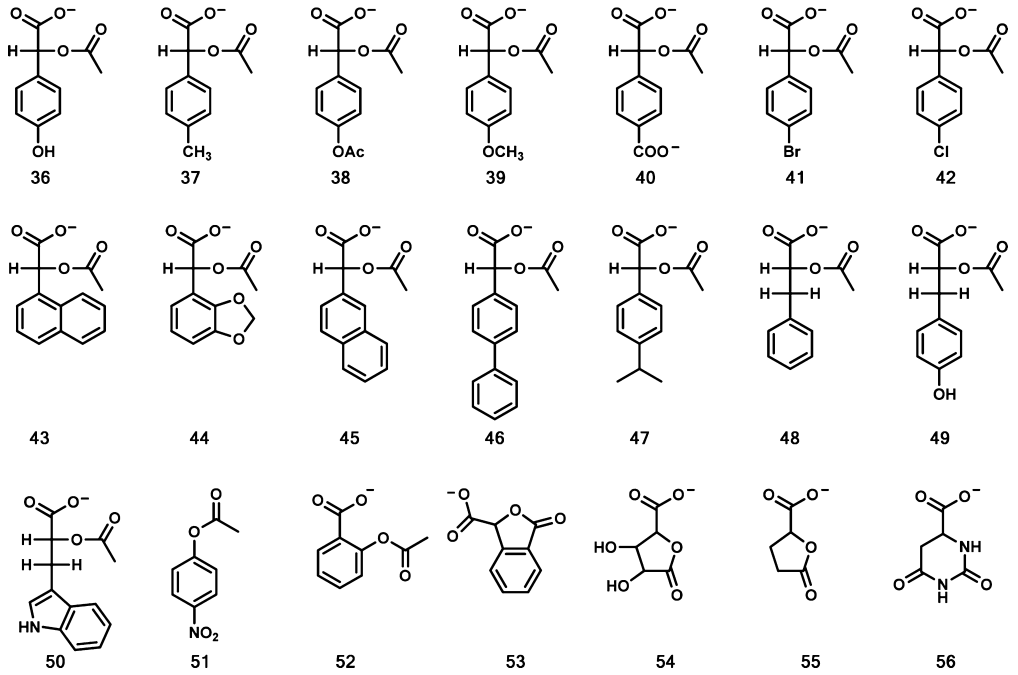

cells. A single colony containing the gene of interest was inoculated into an overnight culture containing 5 mL of LB medium, 100 μg/mL ampicillin, and 20 μg/mL chloramphenicol. The 5 mL starter cultures were used to inoculate 1 L of LB medium. The cells were incubated at 30 °C in a shaker-incubator. When the OD_{600} reached 0.3, the cells were treated

dx.doi.org/10.1021/bi301483z | *Biochemistry* 2013, 52, 228−238

with 150 μM 2,2′-bipyridyl. The cells continued to grow to an OD_{600} of ∼0.6, at which point 200 μM IPTG and 1.0 mM $ZnCl_2$ were added. The temperature was reduced to 20 °C, and the cells were grown overnight for 16 h. The cells where harvested by centrifugation at 8000*g* for 10 min and then frozen at −80 °C. The cell pellet was resuspended in binding buffer containing 20 mM HEPES, 500 mM NaCl, and 5.0 mM imidazole (pH 7.6). The cells were supplemented with 10 μg/mL PMSF and lysed by sonication at 0 °C. The cell debris was removed by centrifugation, and then Atu3266 was purified using a His tag affinity column. The cell lysate supernatant was filtered through a 0.2 μm cellulose acetate sterile filter and loaded onto a Ni^{2+}-NTA column equilibrated with binding buffer. The column was washed with binding buffer until the A_{280} remained constant and below 0.1. The protein of interest was eluted using a gradient from 0 to 500 mM imidazole in a buffer solution containing 10 mM HEPES and 250 mM NaCl (pH 7.6). After dialysis, the protein was judged to be >95% pure by SDS−PAGE.

Protein Concentration and Metal Analysis. The protein concentration was determined spectrophotometrically using a SPECTRAmax-384 PLUS UV−vis spectrophotometer. The concentration was obtained from the absorbance at 280 nm using the extinction coefficients determined from the amino acid sequence (http://web.expasy.org/protparam/). The extinction coefficients for Oant2987 and Atu3266 are 43605 and 43969 M^{-1} cm^{-1}, respectively.[24] The metal content of the purified proteins was determined by inductively coupled plasma emission mass spectrometry (ICP-MS) using a Perkin-Elmer Analyst 700 atomic absorption spectrometer. The samples were prepared by heating 1.0 μM enzyme with 1% (v/v) HNO_3 for 30 min.

Synthesis of Dipeptide Libraries, *N*-Acyl Amino Acids, and Methyl Phosphonates. Syntheses of dipeptide libraries (L-Xaa-L-Xaa, D-Xaa-L-Xaa, and L-Xaa-D-Xaa) and *N*-acetyl, *N*-formyl, and *N*-succinyl derivatives of D- and L-amino acids were conducted as described previously.[25,26] The preparation of the *O*- and *N*-methyl phosphonate derivatives of (*R*)-mandelate (**57**) and D-phenylglycine (**58**), respectively, was conducted as previously described.[25] The structures of these compounds are presented in Scheme 4; their composition was verified by mass spectrometry and nuclear magnetic resonance (NMR).

Scheme 4

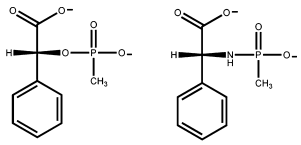

57 58

Screening of *N*-Acyl and Dipeptide Libraries. The preliminary substrate screening of Atu3266 and Oant2987 was initiated by mixing each protein with the N-modified libraries of the D- and L-amino acids (*N*-acetyl, *N*-formyl, and *N*-succinyl) and three dipeptide libraries (L-Xaa-L-Xaa, D-Xaa-L-Xaa, and L-Xaa-D-Xaa). The assays were conducted as previously described.[26] Each assay was buffered with 20 mM HEPES (pH 7.6), and each library contained 17−19 modified amino acids (L- and D-cysteine were not included). Each assay contained each component at ∼100 μM, and 0−1000 nM Atu3266 or Oant2987 was added to initiate the reaction. A negative control was prepared without the addition of either Atu3266 or Oant2987. The initial screening reactions were conducted at 30 °C for 15 h. The formation of free amino acids was detected using a modified Cd-ninhydrin assay.[27] Each 70 μL reaction mixture was quenched with 280 μL of ninhydrin reagent. The entire reaction mixture was developed heating at 85 °C for 15 min and then cooled. A 250 μL aliquot was transferred to a 96-well UV−visible micro plate, and the extent of total free amino acids was measured at 507 nm.

Screening Methods for Deacetylase Activity. All compounds having a hydrolyzable acetyl moiety were screened using the acetic acid kit, KACETAF, from Megazyme. The catalytic activities of Atu3266 and Oant2987 were monitored by the formation of acetate and the subsequent reduction of NAD^+ by the coupled activity of acetyl-coenzyme A synthetase, citrate synthase, and L-malate dehydrogenase. The reaction was monitored spectrophotometrically at 340 nm. The 250 μL reaction mixture contained 1.0 mM test compound, 20 mM HEPES (pH 7.6), and 75 μL of the coupling system containing 128 mM TEA buffer (pH 8.4), 5.0 mM NAD^+, 3.1 mM ATP, 3.2 mM $MgCl_2$, 0.15 mM CoA, 4 units of L-malate dehydrogenase, 0.6 unit of citrate synthase, and 0.3 unit of acetyl-CoA synthetase. Each compound was tested for ester hydrolysis at 30 °C, and the reaction was initiated by the addition of 1.0 μM Atu3266 or Oant2987.

Screening of *O*-Propionyl Compounds. The hydrolysis of (*R*)-3-hydroxy-2-(propionyloxy) propanoate (**21**) and (*R*)-2-(propionyloxy) butanoate (**22**) was assessed using a pH-sensitive colorimetric assay.[28] The hydrolysis of the ester bond releases a proton that was detected using a pH indicator dye, cresol purple. The screening reactions were conducted in 2.5 mM Bicine buffer (pH 8.3) containing 0.2 M NaCl and each compound at 1.0 mM with up to 1.0 μM enzyme. Each reaction mixture contained 0.1 mM cresol purple in 1% DMSO, and the change in absorbance was monitored at 577 nm. The extinction coefficient under these reaction conditions was determined to be 1.51×10^3 M^{-1} cm^{-1} using acetic acid as a titrant.

Data Analysis. The kinetic constants k_{cat}, K_m, and k_{cat}/K_m were determined for Atu3266 and Oant2987 for selected substrates by fitting the initial velocity data to eq 1. Competitive inhibition constants were determined using eq 2 for a competitive inhibitor.

$$v/E_t = (k_{cat}[A])/(K_m + [A]) \quad (1)$$

$$v/E_t = (k_{cat}[A])/[K_m(1 + I/K_{is}) + [A]] \quad (2)$$

where v is the initial velocity, E_t is the enzyme concentration, k_{cat} is the turnover number, [A] is the substrate concentration, K_m is the Michaelis−Menten constant, I is the inhibitor concentration, and K_{is} is the slope inhibition constant.

Crystallization and Structure Determination of Atu3266. Selenomethionine (SeMet)-substituted Atu3266 from *Agrobacterium tumefaciens* with the six-His tag intact was crystallized by mixing 1.5 μL of protein [5 mg/mL in a buffer consisting of 10 mM HEPES (pH 7.5), 150 mM NaCl, 10 mM methionine, 10% glycerol, and 5 mM DTT] with 1.5 μL of a reservoir solution containing 0.1 M HEPES (pH 7.5), 25% PEG 3350, and 0.2 M ammonium sulfate and equilibrating against the same reservoir solution by the hanging drop vapor diffusion method. Crystals appeared after 3 days and were flashed-cooled in liquid nitrogen for data collection.

A native data set and a complete MAD data set from single crystals were collected at 100 K on beamline 31-ID at APS

using a Mar CCD 225 detector. Crystals diffracted to 2.62 Å and belong to orthorhombic space group $P2_12_12_1$ with six molecules in the asymmetric unit. Data were indexed, integrated, and scaled using HKL2000.[29] The selenium substructure was determined using SHELXD.[30] The phase refinement and density modifications were conducted using SHAARP and SOLOMON.[31,32] Model building was conducted using ARP/wARP.[33] Further model building and refinement of the structure were conducted in iterative cycles using O and CNS version 1.1.[34,35] Extra residual density was observed near the NZ atom of Lys-175, and the lysine residue was modeled as a carboxylated lysine. In addition, two zinc ions and one imidazole were located per molecule and included in the later stages of refinement. The atomic coordinates and structure factors for the Atu3266 structure have been deposited in the Protein Data Bank as entry 2OGJ. Crystal, diffraction data, and refinement details are given in Table 1.

Table 1. Data Collection and Refinement Statistics for Atu3266

Data Set and Unit Cell Parameters			
beamline	NSLS X12C		
a (Å)	90.65		
b (Å)	139.2		
c (Å)	206.13		
$\alpha = \beta = \gamma$ (deg)	90		
space group	$P2_12_12_1$		
Data Collection Statistics			
	peak	inflection	remote
wavelength (Å)	0.9793	0.9798	0.94
resolution range (Å)	50−2.6	50−2.8	50−2.8
redundancy	5.8	5.5	5.2
mean $I/\sigma(I)$	14.5	13.2	12.8
R_{merge} [a]	0.121	0.125	0.118
no. of unique reflections	139906	138603	138965
Phasing Statistics			
phasing power[b] (ano)			0.21/0.28
FOM[c] (centric/acentric)			0.85
Refinement Statistics			
resolution range (Å)			2.62−39.7
no. of reflections (work)			139800
no. of reflections (test)			4173
no. of protein atoms			16450
no. of heterogen atoms			22
no. of solvent atoms			113
R_{factor}, R_{free} [d]			0.256, 0.302
root-mean-square deviation for bond lengths (Å)			0.016
root-mean-square deviation for bond angles (deg)			1.6
⟨B values⟩ (Å^2)			58.3
Protein Data Bank entry			2OGJ

[a] $R_{merge} = \sum_j |I_h - \langle I_h \rangle| / \sum I_h$ where $\langle I_h \rangle$ is the average intensity over symmetry equivalents. [b] As defined in SHARP. [c] FOM is the figure of merit as defined by SHARP. [d] $R_{factor} = \sum |F_{obs} - F_{calc}| / \sum |F_{obs}|$. R_{free} is the same as R_{factor} but for the test set.

Computational Docking. A nonredundant virtual library of compounds from the Kyoto Encyclopedia of Genes and Genomes (KEGG) was filtered on the basis of possible amidohydrolase reactions and subsequently prepared as high-energy intermediates (HEIs). The HEI compounds are generated by the addition of an activated water to the metabolite molecules from KEGG, which approximates the transition state with variable substrate protonation states.[9,36] This library contains 6440 unique metabolites that generated 57672 HEI molecules. This virtual HEI library (HEI KEGG) was docked against Atu3266.

The Atu3266 structure was prepared for docking as previously described.[37] All six chains from the asymmetric unit of Atu3266 [Protein Data Bank (PDB) entry 2OGJ] were aligned against chain A, and the best rotamer positions for each amino acid were chosen on the basis of $2F_oF_c$ density maps. For example, the positions of residues 177, 267, and 268 near the active site were chosen on the basis of chain D positions. Histidine protonation states were manually defined in the vicinity of the two zinc ions, directing polar hydrogens away from the binuclear metal center. All other polar hydrogens were automatically generated. The charges on the α- and β-zinc ions were assigned as 1.4 and 1.3, respectively,[37] and the remaining charge difference was distributed to the metal ligating residues [His-77, His-79, His-208, and His-231 (0.25 each); Asp-291 (−0.9); and Kcx-175 (−0.8)] to give each metal an apparent charge of 2.0.

Molecules were docked into the active site of Atu3266 with DOCK version 3.6[38,39] (http://dock.compbio.ucsf.edu/). Docking was performed using receptor and ligand bin sizes of 0.4 Å, an overlap of 0.1−0.2 Å, and a distance tolerance of 1.5 Å with label matching turned off. The docked molecules were subjected to 250 cycles of rigid-body minimization and were scored on the basis of van der Waals, electrostatic, and solvation terms. Each pose of the scored HEI metabolites was filtered, based on a maximal distance of 4 Å between the reactive center of the HEI molecule and the zinc metal center. Finally, the top 500 scored molecules were manually inspected to identify potential substrates. Some of the docked substrates were further subjected to minimization with SZYBKI;[39] this was used to confirm substrate fit and to further investigate hydrogen bond networks.

Because many molecules were synthesized de novo for this project, they were not present in the KEGG library. To investigate the stereospecificity of the compounds hydrolyzed by Atu3266 and Oant2987, a dedicated library (HEI AC) containing all of the experimentally tested compounds (Schemes 2 and 3, compounds **1**−**56**) was generated as previously described for the HEI KEGG library.[9,36] To further identify new ligands, the HEI AC library was expanded to contain other molecules with the acetylated α-hydroxyl carboxylate motif [smiles string O=C(O)C(R_2)OC(=O)C], and molecules with insertions around the chiral carbon {smiles string [O=C(O)X_nC(R_2)X_nOC(=O)X_n]}. These new compounds were docked and scored in the same manner as the HEI KEGG library molecules.

RESULTS

Purification of Atu3266 and Oant2987. Atu3266 was purified to homogeneity, and the identity of this protein was confirmed by sequencing the first eight amino acids from the N-terminus. Oant2987 was purified to homogeneity using gel filtration and anion exchange chromatography. Each protein was >95% pure based on SDS−PAGE analysis. ICP-MS confirmed the presence of 2.0 ± 0.2 equiv of Zn per subunit of Atu3266 and 1.0 ± 0.1 equiv of Zn per subunit of Oant2987 with <0.1 equiv of iron and manganese. The addition of supplemental zinc to Oant2987 did not improve the catalytic hydrolysis of acetyl-(*R*)-mandelate.

dx.doi.org/10.1021/bi301483z | *Biochemistry* 2013, 52, 228−238

Three-Dimensional Structure of Atu3266. The three-dimensional structure of Atu3266 was determined to a resolution of 2.62 Å (PDB entry 2OGJ). The six protomers in the asymmetric unit form a dimer of trimers as illustrated in Figure 2. The hexamer appears as two disks (made of three protomers) stacked against each other. Each protomer consists of two domains: a TIM barrel domain and a second domain consisting of two β-sheets formed by both N- and C-terminal residues as shown in Figure 3. The structure reveals a distorted $(\beta/\alpha)_8$ TIM barrel fold that is similar to those of other structurally characterized enzymes from the AHS.[14] The active site is dominated by a binuclear divalent metal center that is reminiscent of the metal centers found in phosphotriesterase[40] and dihydroorotase[20] as illustrated in Figure 4. The structure of Atu3266 was determined in the presence of imidazole in the active site that is coordinated to the β-metal at a distance of 2.2 Å (not shown). The α-metal is coordinated by His-77 and His-79 at distances of 2.2 and 2.4 Å, respectively. These residues are positioned at the C-terminal end of β-strand 1. This metal ion is also coordinated to Asp-291 from β-strand 8 and a carboxylated Lys-175 (Kcx-175) from β-strand 4. The β-metal is coordinated to the carboxylated lysine from β-strand 4 and to His-208 and His-231 from β-strands 5 and 6. A water molecule is at 3.1 Å from the β-metal ion. The two metal ions are 3.3 Å apart.

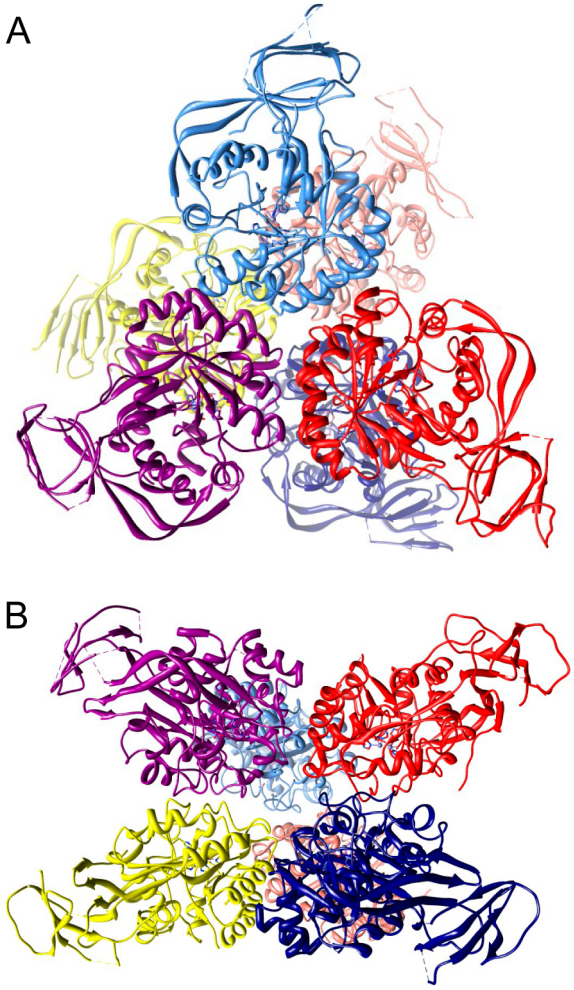

Figure 2. Representation of the hexameric arrangement of subunits for the three-dimensional structure of Atu3266. Face-on (A) and edge-on (B) views of the hexameric structure of PDB entry 2OGJ.

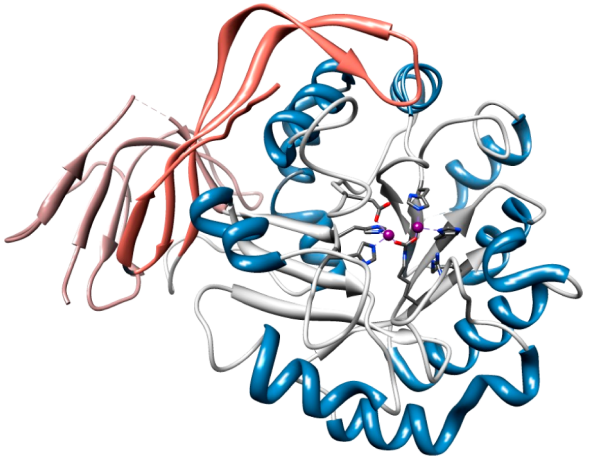

Figure 3. Ribbon representation of the three-dimensional structure domain of Atu3266. The metal-coordinating ligands are colored purple. The central β-barrel is colored gray; the helices are colored blue. Colored rose and tan are the N- and C-terminal domains of the enzyme, respectively.

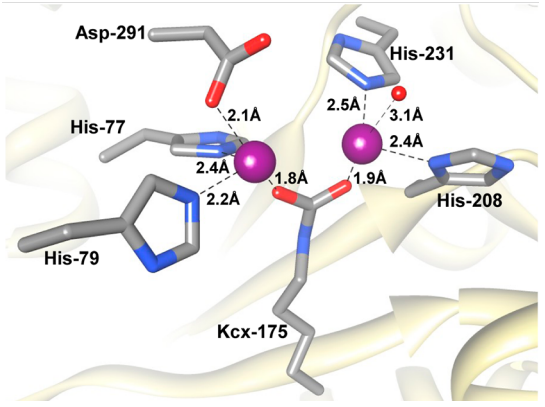

Figure 4. Structural model for the active site of Atu3266 showing the residues that coordinate the binuclear metal center. The metal-ligating residues are colored gray; the binuclear metal center is colored magenta, and the coordinating water molecule to the β-metal is colored red.

Substrate Specificity of Atu3266 and Oant2987. D- and L-dihydroorotate (**56**) were the first two compounds to be tested as substrates for Atu3266, because this enzyme has been annotated in various databases as a dihydroorotase. However, no hydrolysis of these compounds could be observed, and thus, this annotation is not correct. This experiment was followed by the utilization of a focused library of *N*-acetyl, *N*-succinyl, and *N*-formyl derivatives of the common D- and L-amino acids and multiple libraries of L-Xaa-L-Xaa, L-Xaa-D-Xaa, and D-Xaa-L-Xaa dipeptides. From the more than 1200 compounds tested in the initial screening, only two compounds were found with very weak rates of hydrolysis. The values of k_{cat}/K_m for *N*-acetyl-D-serine (**1**) and *N*-acetyl-D-threonine (**2**) are 4.0 and 2.0 M^{-1} s^{-1}, respectively. This finding prompted the separate synthesis of *N*-acetyl-D-cysteine (**3**) and *N*-formyl-D-serine (**4**), but these compounds were not detectable substrates for Atu3266. Methylating the α-carboxylate (compound **5**) or phosphorylating the side chain hydroxyl (compound **6**) of the weak substrate, *N*-acetyl-D-serine, abolished the catalytic activity. The

dx.doi.org/10.1021/bi301483z | *Biochemistry* 2013, 52, 228−238

Table 2. Kinetic Parameters for Atu3266 and Oant2987[a]

	Atu3266			Oant2987		
substrate	k_{cat} (s^{-1})	K_m (mM)	k_{cat}/K_m (M^{-1} s^{-1})	k_{cat} (s^{-1})	K_m (mM)	k_{cat}/K_m (M^{-1} s^{-1})
1	na	na	4	nc	nc	nc
2	na	na	2	nc	nc	nc
3	<0.001	na	na	<0.001	na	na
9	12 ± 1	25 ± 4	(4.8 ± 0.1) × 10^2	0.6 ± 0.1	2.1 ± 0.5	(3 ± 1) × 10^2
13	40 ± 3	3.1 ± 0.5	(1.3 ± 0.2) × 10^4	4.2 ± 0.2	1.1 ± 0.2	(4.2 ± 0.8) × 10^3
14	0.8 ± 0.1	0.5 ± 0.1	(1.6 ± 0.2) × 10^3	0.4 ± 0.1	0.6 ± 0.1	(7 ± 1) × 10^2
15	0.5 ± 0.1	10 ± 2	50 ± 10	na	na	40
16	0.6 ± 0.1	9.5 ± 0.7	58 ± 6	na	na	60
17	1.5 ± 0.1	7 ± 1	(2.1 ± 0.3) × 10^2	na	na	200
18	3.1 ± 0.3	6 ± 1	(5.0 ± 0.8) × 10^2	0.81 ± 0.08	1.2 ± 0.1	(8.1 ± 0.8) × 10^3
19	1.1 ± 0.2	9.5 ± 3.0	(1.2 ± 0.4) × 10^2	0.23 ± 0.02	1.4 ± 0.1	(2.2 ± 0.2) × 10^2
20	0.41 ± 0.04	2.1 ± 0.5	(2.0 ± 0.5) × 10^2	0.30 ± 0.02	0.71 ± 0.02	(4.3 ± 0.4) × 10^2
21	na	na	(1.1 ± 0.6) × 10^2	na	na	30
22	na	na	(1.8 ± 0.6) × 10^2	na	na	30
23	na	na	50 ± 10	nc	nc	nc
24	na	na	(2.4 ± 0.5) × 10^2	2.0 ± 0.1	2.0 ± 0.5	(1.0 ± 0.2) × 10^3
25	0.10 ± 0.03	0.4 ± 0.1	(2.5 ± 0.2) × 10^2	<0.05	na	na
26	0.21 ± 0.01	0.3 ± 0.1	(6.6 ± 1.0) × 10^2	<0.02	na	na
27	2.3 ± 0.2	30 ± 10	67 ± 22	na	na	40
28	280 ± 5	1.0 ± 0.1	(2.8 ± 0.2) × 10^5	130 ± 1	0.7 ± 0.1	(1.8 ± 0.2) × 10^5
36	34 ± 2	1.1 ± 0.1	(3.4 ± 0.3) × 10^4	6.0 ± 0.2	0.21 ± 0.02	(3.0 ± 0.3) × 10^4
37	70 ± 7	7 ± 1	(1.0 ± 0.1) × 10^4	60 ± 4	3.4 ± 0.5	(1.7 ± 0.2) × 10^4
38	43 ± 5	4 ± 1	(1.1 ± 0.2) × 10^4	4.1 ± 0.3	0.5 ± 0.1	(8.0 ± 0.8) × 10^3
39	30 ± 9	10 ± 3	(3.0 ± 0.9) × 10^3	60 ± 6	18 ± 2	(3.3 ± 0.3) × 10^3
40	na	na	(3.0 ± 0.3) × 10^3	50 ± 5	5 ± 1	(1.0 ± 0.2) × 10^4
41	na	na	(5.0 ± 0.4) × 10^3	36 ± 5	8 ± 1	(4.5 ± 0.5) × 10^3
42	190 ± 20	12 ± 3	(1.6 ± 0.1) × 10^4	150 ± 10	3.0 ± 0.5	(5 ± 1) × 10^4
43	na	na	(2.2 ± 0.2) × 10^3	30 ± 2	4.0 ± 0.5	(7.5 ± 0.9) × 10^3
44	na	na	(1.0 ± 0.1) × 10^3	50 ± 1	5 ± 1	(1.0 ± 0.2) × 10^4
45	10 ± 1	2.0 ± 0.2	(5.0 ± 0.5) × 10^3	40 ± 5	11 ± 3	(3.6 ± 0.9) × 10^3
46	7.0 ± 0.2	0.6 ± 0.1	(1.0 ± 0.1) × 10^4	10 ± 1	0.8 ± 0.2	(1.2 ± 0.3) × 10^4
47	10 ± 1	1.4 ± 0.3	(7.0 ± 0.2) × 10^3	20 ± 2	2.0 ± 0.5	(1.0 ± 0.2) × 10^4
48	50 ± 4	10 ± 1	(5.1 ± 0.1) × 10^3	60 ± 6	9 ± 1	(7.0 ± 0.7) × 10^3
49	90 ± 9	7 ± 1	(1.3 ± 0.1) × 10^4	80 ± 6	3 ± 0.2	(2.7 ± 0.2) × 10^4
50	17 ± 3	5 ± 1	(3.5 ± 0.1) × 10^3	28 ± 10	na	(1 ± 0.3) × 10^3

[a]nc denotes a parameter that was not calculated, mainly because there was no detection of acetic acid by the coupling system, whereas na denotes a parameter that was not available, in the event that the substrate did not saturate the enzyme and the rates obtained were fit to a linear curve to obtain V/K for the observed activity.

N-carbamoyl (compound **7**) and *N*-phosphoryl (compound **8**) derivatives of D-serine were not catalytically active. However, the substitution of the α-amino group with an α-hydroxyl group, as in 2-acetyl-(*R*)-glycerate (**9**), resulted in a 2 order of magnitude improvement in k_{cat}/K_m, relative to that of *N*-acetyl-D-serine.

The dramatic increase in the rate of hydrolysis of 2-acetyl-(*R*)-glycerate (**9**) prompted the exploration of modifications to this substructure. However, 2-phospho-(*R*)-glycerate (**10**) and 3-phospho-2-acetyl-(*R*)-glycerate (**11**) were not hydrolyzed, and no activity could be observed with 2-acetylglycerol (**12**). Surprisingly, excision of the hydroxymethyl substituent to form acetyl glycolate (**13**) increased k_{cat}/K_m by a factor of 27, relative to that of compound **9**. Further substitutions to the substructure of acetyl glycolate (**13**) did not result in any further improvements (compounds **14**–**28**) in catalytic activity except for the addition of a phenyl group. Acetyl-(*R*)-mandelate (**28**) is hydrolyzed with a k_{cat}/K_m of 2.8 × 10^5 M^{-1} s^{-1}. This is a factor of 20 better than that of acetyl glycolate (**13**) and nearly 5 orders of magnitude better than that of the initial hit, *N*-acetyl-D-serine (**1**). No activity was observed with phosphoenolpyruvate (**30**), the amide of acetyl-(*R*)-mandelate (**31**), 2-phospho-(*R*)-mandelate (**32**), acetyl-D-phenylglycine (**33**), the methyl ester of acetyl-(*R*)-mandelate (**34**), acetyl-(*S*)-mandelate (**35**), or 2-acetoxyisobutyric acid (**29**). Further modifications to acetyl-(*R*)-mandelate did not improve the rate of hydrolysis (see compounds **36**–**50**), relative to that of acetyl-(*R*)-mandelate (**28**). Other modifications, including *p*-nitrophenyl acetate (**51**), aspirin (**52**), and various lactones (**53**–**55**), were not active. The kinetic constants for the catalytically active substrates are listed in Table 2.

Inhibition by *N*-Methyl Phosphonate of D-Phenylglycine. The *N*-methylphosphonate and *O*-methylphosphonate derivatives of D-phenylglycine (**57**) and *R*-mandelate (**56**), respectively, were synthesized and tested as inhibitors for the hydrolysis of acetyl-(*R*)-mandelate (**28**) by Atu3266 and Oant2987. The *O*-methylphosphonate inhibitor of (*R*)-mandelate was unstable. However, the *N*-methylphosphonate analogue of D-phenylglycine (**57**) was found to be a competitive inhibitor versus acetyl-(*R*)-mandelate. A fit of the

dx.doi.org/10.1021/bi301483z | *Biochemistry* 2013, 52, 228–238

data to eq 2 gave inhibition constants of 35 ± 2 μM for Atu3266 and 40 ± 2 μM for Oant2987.

Computational Docking to the Active Site of Atu3266. Molecules from the HEI KEGG library consisted of high-quality poses enriched for carbamoylated and acetylated amino acids. Thus, acetylated amino acids such as *N*-acetyl-L-lysine (rank of 40), *N*-acetyl-D-methionine (rank of 171), *N*-acetyl-D-cysteine (**3**) (rank of 218), *N*-acetyl-L-leucine (rank of 313), and *N*-acetyl-D-phenylalanine (**48**) (rank of 440) (Figure S1 of the Supporting Information) and other metabolites such as *N*-carbamoyl-L-aspartate, *N*-acetyl-D-glucosaminate, and oxalureate were found at the top of the docking list. Further virtual docking experiments with the HEI AC library suggested a common binding pose for the compounds that contain the HEI acetylated α-hydroxyl carboxylate (Figure 5A). A detailed

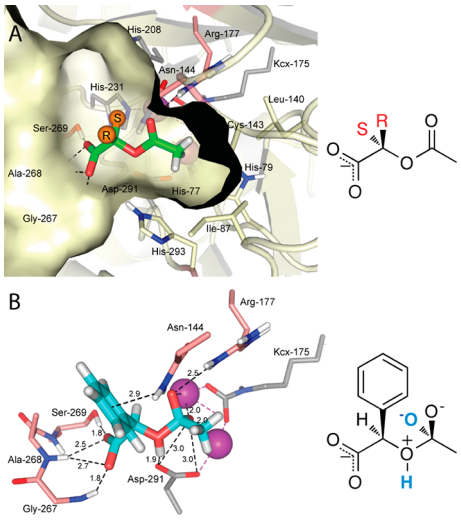

Figure 5. Modeled structure of docked acetyl-(*R*)-mandelate into the active site of Atu3266. On the basis of the docking results of the HEI library, panel A is a model of the ground state acetylated α-hydroxyl carboxylate substrates (green sticks) in the active site. The orange spheres illustrate the possible orientation of the *R*- and *S*-enantiomers. The active site is shown as a surface representation; hydrogen bonds between the carboxylate of the substrate and loop 267−269 are shown as dashed lines. In this orientation, the bridging oxygen of the ester points toward Asp-291 and the carbonyl oxygen stacks over the binuclear metal center (purple spheres), directing the methyl group of the acetate into a hydrophobic pocket lined by Ile-87, Leu-140, Cys-142, His-79, and His-293. (B) The HEI substrate, acetyl-(*R*)-mandelate (**28**) (cyan sticks) (rank of 221), is shown in its best docked pose. Here the hydrogen on the bridging oxygen is 1.9 Å from Asp-291. The HEI intermediate is stabilized by Arg-177. The carboxylate hydrogen bonds with loop 267−269, and the phenyl group is positioned between the cavity walls, allowing for stacking interactions with Asn-144.

examination revealed that the acetylated α-hydroxyl carboxylates direct the ester group toward the metal cluster, where the carbonyl oxygen is positioned over the α- and β-zinc atoms and the transition state is stabilized by Arg-177 (Figure 5B). In this orientation, the methyl group of the acetyl moiety is surrounded by the hydrophobic pocket lined by Ile-87, Leu-140, Cys-142, and the plane of the imidazole side chain of His-79 and His-293. This hydrophobic pocket is large enough that it can accommodate an ethyl group such as that of (*R*)-propionyloxy mandelate (rank of 241) (Figure S2i of the Supporting Information). The bridging oxygen of the ester moiety is oriented toward Asp-291, thus facilitating the enzymatic hydrolysis of the acetylated α-hydroxyl carboxylates.

The docking calculations indicate that the two remaining fragments of the molecule, the carboxylate and the mostly nonpolar substituent at the chiral carbon, are necessary for the correct binding and orientation of the substrates in the active site. Critical to the binding is the carboxylate, which forms a hydrogen bond network with the loop formed between β-strand 7 and α-helix 7 of the AHS domain. These hydrogen bond interactions include the amide nitrogens of Gly-267 and Ala-268, and the hydroxyl side chain of Ser-269. In some instances, an additional hydrogen bond is formed between the carboxylate of the substrate and the Nε hydrogen of His-293. The second and more variable portions of the substrates for Oant2987 and Atu3266 contain mostly nonpolar substitutions at the chiral α-carbon of the acetylated α-hydroxyl carboxylates. All molecules identified as substrates possess the *R*-stereochemistry at C2 of the acetylated α-hydroxyl carboxylates, including the best substrate, acetyl-(*R*)-mandelate (**28**). The catalytically competent pose of the transition state mimic for acetyl-(*R*)-mandelate (**28**) identified from the HEI AC library had an energy score of −140.65. Thus, this molecule would have ranked 221 out of 57672 HEI KEGG molecules, placing it in the 99.6th percentile. In this pose, the aromatic phenyl ring moiety of acetyl-(*R*)-mandelate (**28**) provides a π-stacking interaction with the side chain nitrogen atom of Asn-144. The distance between these two components varies depending on the substrates docked; however, in the catalytically competent poses, these molecules adopt conformations where the center of the ring is 2.8−3.5 Å from the amino acid side chain.[41]

With the HEI AC virtual library, we have been able to screen compounds with slightly longer backbones (insertions around the chiral carbon). Docking results suggest that larger molecules can be accommodated into the active site, such as *O*-acetyl-(*S*)-carnitine, (*S*)-3-acetoxy-4-(dimethylamino)-butanoic acid, acetyltropic acid, and 3-carbamoyloxy-2-phenyl-propionic acid (Figure S3a of the Supporting Information). Of these, (*S*)-3-acetoxy-4-(dimethylamino)butanoic acid (Figure S3b of the Supporting Information) and racemic acetyltropic acid (Figure S3c of the Supporting Information) were tested as possible substrates for Atu3266. However, only acetyltropic acid is active, albeit with a very poor k_{cat}/K_m of 200 M^{-1} s^{-1}. This indicates that a small extension between the chiral carbon and the ester can be tolerated, but the simple acetylated hydroxyl carboxylate chemotype is preferred.

DISCUSSION

Three-Dimensional Structure of Atu3266. The three-dimensional structure of Atu3266 shows that this enzyme possesses a binuclear metal center, reminiscent of other enzymes in the amidohydrolase superfamily such as dihydroorotase, phosphotriesterase, and urease.[13] The buried α-metal is coordinated by His-77, His-79, Asp-291, and carboxylated Lys-175. The more solvent-exposed β-metal is coordinated to His-208, His-231, carboxylated Lys-175, and a water molecule. The individual subunits of Atu3266 associate to form a hexameric oligomer.

cog3964. There are 24 clusters of orthologous groups in the AHS, and cog3964 is one of the smallest, with ∼200 sequences (Figure 1). The most common annotation in NCBI for this cluster of enzymes is dihydroorotase and, in some cases, adenine deaminase. The basis for this annotation is not clear, but the experiments reported here demonstrate that this

dx.doi.org/10.1021/bi301483z | *Biochemistry* 2013, 52, 228−238

annotation is incorrect. When the *E* value cutoff is set to 10^{-70}, the sequence similarity network for cog3964 segregates into eight groups with three or more sequences per group and Atu3266 and Oant2987 belong to Group 6 of cog3964. An amino acid sequence comparison between those enzymes in Group 6 of cog3964 and the structurally characterized dihydroorotases and adenine deaminases (not shown) demonstrates that the key residues that have been implicated in substrate binding and recognition in these enzymes are not present in either Atu3266 or Oant2987. This supports the conclusion that Atu3266 and Oant2987 do not catalyze the deamination of adenine or the hydrolysis of dihydroorotate.

Determination of the Substrate Profile. The first indication of catalytic activity by Atu3266 was observed in a library of *N*-acetyl D-amino acids. After each component of the library had been tested independently, it was observed that *N*-acetyl-D-serine (4 M^{-1} s^{-1}) and *N*-acetyl-D-threonine (2 M^{-1} s^{-1}) were the only compounds in the *N*-acetyl-D-Xaa library to be hydrolyzed. Screening for hydrolytic activity was also conducted using a comprehensive library of dipeptides; however, none of the dipeptide libraries showed detectable catalytic activity. Subsequently, we focused on the activity obtained from *N*-acetyl-D-serine and developed a library of compounds with various modifications, including changes in stereochemistry at the central α-chiral carbon, the side chain, and carboxylate functionalities. None of these changes generated a better substrate. However, when the amide linkage was changed to an ester, a 100-fold increase in activity was observed. Atu3266 hydrolyzes the ester linkage of acetyl-(*R*)-glycerate with a rate constant of 400 M^{-1} s^{-1}. When the hydroxymethyl group was removed and replaced with a hydrogen (acetyl glycolate), the rate of hydrolysis increased by an additional 2 orders of magnitude (1.3×10^4 M^{-1} s^{-1}). The highest activity was achieved in the deacetylation of acetyl-(*R*)-mandelate with a rate constant of 2.8×10^5 M^{-1} s^{-1}.

Additional modifications to the acetyl-(*R*)-mandelate substructure failed to improve the catalytic activity. Substitutions and modifications to the C1 carboxylate eliminated deacetylation activity. These alterations included methyl ester and amide formation, phosphorylation, and reduction to a hydroxy methyl group. At C2, the most beneficial modification was the change of the amide nitrogen to oxygen to form an ester. Modification of the acetyl group to a formyl, succinyl, or carbamoyl group did not reveal any of the three were a better substituent than the acetyl group. The stereochemistry at C2 must be *R*. The acetyl group could be extended to a propionyl group, but the rate of hydrolysis is reduced. The presence of the phenyl group at the side chain position proved to be the best substitution, but addition of functionality to the aromatic ring decreased the rate of hydrolysis.

The organisms containing Atu3266 and Oant2987 are devoid of other genes that are obvious candidates for the metabolism of mandelate. However, most of the organisms that contain a protein from cog3964 also have an adjacent gene that is an apparent homologue to selenocysteine synthase (SelA) that belongs to cog1921. The genes for two of the proteins (Atu3263 and Oant2990) were cloned and expressed, and the proteins were purified to homogeneity (data not shown). The purified enzymes contained pyridoxal 5′-phosphate, but we were unable to identify any catalytic activity for these proteins with a library of amino acids. The relationship between the proteins from cog1921 and cog3964 is not obvious.

Comparisons to Other *N*-Acetyl D-Amino Acid Deacetylases. Other enzymes within the amidohydrolase superfamily have been shown to catalyze the hydrolysis of *N*-acetyl D-amino acid derivatives. For example, enzymes within cog3653 have been shown to be *N*-acetyl D-amino acid deacetylases.[26,42−44] In cog3653, the binuclear metal center is not bridged by a carboxylated lysine residue and the α-carboxylate group of the substrate is ion paired and hydrogen bonded to conserved arginine and tyrosine residues.[26] These motifs are not conserved in the enzymes of cog3964, where instead the carboxylate group of the substrate is recognized by the backbone residues following β-strand 7.

At this point, it is not clear whether the enzymes identified in this investigation from cog3964 are generic esterases or whether there is a more specific substrate. Acetyl-(*R*)-mandelate has apparently not been identified as a physiological metabolite in bacteria. In those organisms that have been found to use mandelate as a carbon source, there is no indication of a requirement of a deacetylase for the hydrolysis of acetyl-(*R*)-mandelate.[45]

Computational Docking for Identification of Substrate−Enzyme Interactions. Docking of the HEI KEGG virtual metabolite library to the Atu3266 structure was highly enriched for carbamoylated or acetylated amino acids (acetyl-Met, -Cys, -Phe, -Leu, and -Lys) (Figure S1 of the Supporting Information). An examination of the KEGG database revealed that the database included only 10 acetylated amino acids (Met, Cys, Phe, Leu, Lys, His, Trp, Asp, Glu, and Gln). This indicates a high degree of enrichment in the docking list for the *N*-acetyl amino acids as five of them were found in the top 0.76% of the overall pool of HEI KEGG compounds. As such, the initial docking experiments with the HEI KEGG library did not include the two catalytically competent acetylated amino acids, *N*-acetyl-D-serine (**1**) and *N*-acetyl-D-threonine (**2**). These were subsequently prepared and docked in the HEI AC library and yielded scores that would rank them 321st and 265th, respectively, out of 57672 HEI KEGG molecules. The poses of the two amino acids are suboptimal as they either leave the side chain hydroxyl unsatisfied or allow it to partially interact with the carboxylate binding loop. However, other N-acetylated amino acids are found to optimally occupy the active site, as seen with *N*-acetyl-D-phenylglycine (**33**) (Figure S4 of the Supporting Information).

On the basis of the analysis of the focused HEI AC library docking results, molecules that are turned over by the enzyme contain an acetylated α-hydroxyl carboxylate that positions the acetyl moiety over the zinc atoms, directing the methyl group into a small hydrophobic pocket. This pocket is large enough to accommodate ethyl groups as seen by the substrate (*R*)-propionyloxy mandelate (Figure S2i of the Supporting Information) and (*R*)-2-(propionyloxy) butanoate (**22**) (Figure S2b of the Supporting Information). In addition, this catalytically competent pose orients the carboxylate of the substrate toward the loop formed by Gly-267, Ala-268, and Ser-269 (Figure 5A). In this pose, any substitutions or bulky additions on the substrate carboxylate would change the electrostatics or cause steric clashes, precluding binding. For example, molecules with an addition of a methyl group to form an ester (**34**) or molecules with a substitution of the carboxylate with an organic amide (**31**) demonstrate no enzymatic activity.

Further docking indicates a preference for the *R*-enantiomer of the acetylated α-hydroxyl carboxylates, such as acetyl-(*R*)-

mandelate (**28**). The *R*-enantiomers direct the hydrogen of the chiral carbon toward the floor of the active site cavity and provide ample space for the substituent (Figure 5B) while still orienting the bridging oxygen with ideal geometry and distance from Asp-291 and thus facilitating catalysis. On the basis of the well-positioned docking poses of the substrates, we can infer from the HEI docked molecules that the ground state *R*-enantiomers could easily enter the active site in the extended conformation (Figure 5A). In this conformation, the ligands could easily be subjected to nucleophilic attack by an activated water molecule. Substrates that contain the *R*-enantiomer can easily accommodate bulky substituents, such as the phenyl ring of acetyl-(*R*)-mandelate (**28**), and even larger hydrophobic groups (**37**, **43**, and **46**) (Figure S2d,g,h,k of the Supporting Information), which fit into the active site between the cavity walls. Furthermore, compounds with aromatic rings engage in perpendicular π-stacking interactions with the side chain nitrogen atom of Asn-144. This interaction is not present in the small branched or cyclohexane-containing compounds (**13**, **14**, **18**, **19**, **22**, **24**−**27**, and **48**−**50**), which may explain the difference in affinity parameters. This is illustrated by the different binding modes and interactions of (*R*)-2-acetoxybutanoic acid (**18**) and (*R*)-2-acetoxy-2-cyclohexylacetate acid (**27**) (Figure S2a,j of the Supporting Information). Only a few ionic interactions are observed for charged substituents on the acetylated α-hydroxyl carboxylates; these charged interactions are with Asn-144 (Figure S2f,l of the Supporting Information) and Lys-236 (Figure S2c,e of the Supporting Information) for some of the substrates.

Strategy for Functional Annotation. The functional annotation of Atu3266 as an enzyme that is able to catalyze the hydrolysis of an ester linkage from substituted α-hydroxyl carboxylates with *R*-stereochemistry began with the identification of the weak substrate, *N*-acetyl-D-serine. The combination of focused chemical libraries and computational docking to the three-dimensional crystal structure resulted in the identification of acetyl-(*R*)-mandelate as a substrate that was 5 orders of magnitude better than the initial hit. In addition to Oant2987, we predict that seven other enzymes from Group 6 of cog3964 will have the same substrate profile as Atu3266. These proteins are listed in Table S1 of the Supporting Information. The identification of function for Group 6 of cog3964 will facilitate the functional annotation for the additional groups of proteins in this COG. In preliminary experiments, a protein from Group 2 of cog3964 has been purified and crystallized (EF0837 from *Enterococcus faecalis*, gil 29375425, PDB entry 2ICS). The sequence of this protein is 35% identical with that of Atu3266, and EF0837 catalyzes the hydrolysis of acetyl-(*R*)-mandelate with a k_{cat}/K_m value that is 3 orders of magnitude smaller than the value observed for Atu3266 and Oant2987. These results suggest that the substrate profile for this enzyme will be different from that of Atu3266. Efforts to identify the substrate for the enzymes of Group 2 are currently underway.

■ ASSOCIATED CONTENT

Supporting Information

Synthetic procedures for the preparation of the compounds used in this investigation and additional figures and tables. This material is available free of charge via the Internet at http://pubs.acs.org.

Accession Codes

The X-ray coordinates and structure factors for Atu3266 have been deposited in the Protein Data Bank as entry 2OGJ.

■ AUTHOR INFORMATION

Corresponding Author

*S.S.: telephone, (631) 344-3187; fax, (631) 344-3407; e-mail, swami@bnl.gov. B.K.S.: telephone, (415) 514-4126; fax, (415) 514-4260; e-mail, shoichet@cgl.ucsf.edu. F.M.R.: telephone, (979) 845-3373; fax, (979) 845-9452; e-mail, raushel@chem.tamu.edu.

Funding

This work was supported in part by the Robert A. Welch Foundation (A-840) and the National Institutes of Health (GM 71790 and GM 74945).

Notes

The authors declare no competing financial interest.

■ ACKNOWLEDGMENTS

We thank Dr. Peter Kolb and Dr. Ryan G. Coleman for technical discussions relating to computational techniques.

■ REFERENCES

(1) Roberts, R. J. (2004) Identifying protein function: A call for community action. *PLoS Biol. 2*, E42.

(2) Rost, B., Liu, J., Nair, R., Wrezeszczynski, K. O., and Ofran, Y. (2003) Automatic prediction of protein function. *Cell. Mol. Life Sci. 60*, 2637−2650.

(3) Freidberg, I. (2006) Automated protein function prediction: The genomic challenge. *Briefings Bioinf. 7*, 225−242.

(4) Glasner, M., Gerlt, J. A., and Babbitt, P. C. (2006) Evolution of enzyme superfamilies. *Curr. Opin. Chem. Biol. 10*, 492−497.

(5) Newton, R. J., Griffin, L. E., Bowles, K. M., Meile, C., Gifford, S., Givens, C. E., Howard, E. C., King, E., Oakley, C. A., Risch, C. R., Rinta-Kanto, J., Sharma, S., Sun, S., Varaljay, V., Vila-Costa, M., Westrich, J. R., and Moran, M. A. (2010) Genome characteristics of a generalist marine bacterial lineage. *ISME J. 4*, 784−798.

(6) Sweetlove, L. J., and Fernie, A. R. (2005) Regulation of metabolic networks: Understanding metabolic complexity in the systems biology era. *New Phytol. 168*, 9−24.

(7) Pellegrini, M., Marcotte, E. M., Thompson, M. J., Eisenberg, D., and Yeates, T. O. (1999) Assigning protein functions by comparative genome analysis: Protein phylogenetic profiles. *Proc. Natl. Acad. Sci. U.S.A. 96*, 4285−4288.

(8) Kim, S.-H. (2000) Structural genomics of microbes: An objective. *Curr. Opin. Biol. 10*, 380−383.

(9) Hermann, J. C., Ghanem, E., Li, Y., and Raushel, F. M. (2006) Predicting substrates by docking high-energy intermediates to enzyme structures. *J. Am. Chem. Soc. 128*, 15882−15891.

(10) Kolb, P., Ferreira, R. S., Irwin, J. J., and Shoichet, B. K. (2009) Docking and chemoinformatic screens for new ligands and targets. *Curr. Opin. Biochem. 20*, 429−436.

(11) Senisterra, G. A., Markin, E., Yamazaki, K., Hui, R., Vedadi, M., and Awrey, D. E. (2006) Screening for ligands using a generic and high-throughput light-scattering-based assay. *J. Biomol. Screening 11*, 940−948.

(12) Galperin, M. Y., and Koonin, E. V. (2010) From complete genome sequence to 'complete' understanding? *Trends Biotechnol. 28*, 398−406.

(13) Holm, L., and Sander, C. (1997) An evolutionary treasure: Unification of a broad set of amidohydrolases related to urease. *Proteins 28*, 72−82.

(14) Seibert, C. M., and Raushel, F. M. (2005) Structural and catalytic diversity within the amidohydrolase superfamily. *Biochemistry 44*, 6383−6391.

(15) Li, T., Iwaki, H., Fu, R., Hasegawa, Y., Zhang, H., and Liu, A. (2006) α-Amino-β-carboxymuconic-ε-semialdehyde decarboxylase (ACMSD) is a new member of the amidohydrolase superfamily. *Biochemistry 45*, 6628−6634.
(16) Hara, H., Masai, E., Katayama, Y., and Fukuda, M. (2000) The 4-oxalomesaconate hydratase gene, involved in the protocatechuate 4,5-cleavage pathway, is essential to vanillate and syringate degradation in *Sphingomonas paucimolbilis* SYK-6-hydration reaction. *J. Bacteriol. 182*, 6950−6957.
(17) Williams, L., Nguyen, T., Si, Y., Porter, T., and Raushel, F. M. (2006) Uronate isomerase: A nonhydrolytic member of the amidohydrolase superfamily with an ambivalent requirement for divalent metal ion. *Biochemistry 45*, 7453−7462.
(18) Tatusov, R. L., Galperin, M. Y., Natale, D. A., and Koonin, E. V. (2000) The COG database: A tool for genome-scale analysis of protein functions and evolution. *Nucleic Acids Res. 28*, 33−36.
(19) Tatusov, R. L., Natale, D. A., Garkavtsev, I. V., Tatusova, T. A., Shankavaram, U. T., Rao, B. S., Kiryutin, B., Galperin, M. Y., Federova, N. D., and Koonin, E. V. (2001) The COG database: New developments in phylogenetic classification of proteins from complete genomes. *Nucleic Acids Res. 29*, 22−28.
(20) Thoden, J. B., Phillips, G. N., Neal, T. M., Raushel, F. M., and Holden, H. M. (2001) Molecular structure of dihydroorotase: A paradigm for catalysis through the use of a binuclear metal center. *Biochemistry 40*, 6989−6997.
(21) Porter, T. N., Li, Y., and Raushel, F. M. (2004) Mechanism of the dihydroorotase reaction. *Biochemistry 43*, 16285−16292.
(22) Kamat, S. S., Bagaria, A., Kumaran, D., Holmes-Hampton, G. P., Fan, H., Sali, A., Sauder, M. J., Burley, S. K., Lindahl, P. A., Swaminathan, S., and Raushel., F. M. (2011) Catalytic mechanism and three-dimensional structure of adenine deaminase. *Biochemistry 50*, 1917−1927.
(23) Goble, A. M., Zhang, Z., Sauder, M. J., Burley, S. K., Swaminathan, S., and Raushel, F. M. (2011) Pa0148 from *Pseudomonas aeruginosa* catalyzes the deamination of adenine. *Biochemistry 50*, 6589−6597.
(24) Pace, C. N., Vajdos, F., Fee, L., Grimsley, G., and Gray, T. (1995) How to measure and predict the molar absorption coefficient for a protein. *Protein Sci. 4*, 2411−2423.
(25) Xiang, D., Patskovsky, Y., Chengfu, X., Meyer, A. J., Sauder, J. M., Burley, S. K., Almo, S. C., and Raushel, F. M. (2009) Functional identification of incorrectly annotated prolidases from the amidohydrolase superfamily of enzymes. *Biochemistry 48*, 3730−3742.
(26) Cummings, J. A., Fedorov, A. A., Xu, C., Brown, S., Fedorov, E., Babbitt, P. C., Almo, S. C., and Raushel, F. M. (2009) Annotating enzymes of uncertain function: The deacylation of D-amino acids by members of the amidohydrolase superfamily. *Biochemistry 48*, 6469−6481.
(27) Doi, E., Shibata, D., and Matoba, T. (1981) Modified colorimetric ninhydrin methods for peptidase assay. *Anal. Biochem. 118*, 173−184.
(28) Chapman, E., and Wong, C. H. (2002) A pH sensitive colorimetric assay for the high-throughput screening of enzyme inhibitors and substrates: A case study using kinases. *Bioorg. Med. Chem. 10*, 551−555.
(29) Otwinowski, Z., and Minor, W. (1997) Processing of X-ray diffraction data collected in oscillation mode. *Methods Enzymol. 276*, 307−326.
(30) Schneider, T. R., and Sheldrick, G. M. (2002) Substructure solution with SHELXD. *Acta Crystallogr. D58*, 1772−1779.
(31) Collaborative Computational Project, Number 4 (1994) CCP4 Suite: Programs for protein crystallography. *Acta Crystallogr. D50*, 760−763.
(32) De-La-Fortelle, E., and Bricogne, G. (1997) Maximum-likelihood heavy atom parameter refinement in the MIR and MAD methods. *Methods Enzymol. 276*, 472−493.
(33) Perrakis, A., Morris, R., and Lamzin, V. S. (1999) Automated protein model building combined with iterative structure refinement. *Nat. Struct. Biol. 6*, 458−463.
(34) Brunger, A. T., Adams, P. D., Clore, G. M., Delano, W. L., Gros, P., Grosse-Kunstleve, R. W., Jiang, F. S., Kuszwewski, J., Nilges, M., Pannu, N. S., Read, R. J., Rice, L. M., Somonsom, T., and Warren, G. L. (1998) Crystallography & NMR system: A new software suite for macromolecular structure determination. *Acta Crystallogr. D54*, 905−921.
(35) Jones, T. A., Zou, J.-Y., Cowan, S. W., and Kjeldgaard, M. (1991) Improved methods in building protein models in electron density map and the location of errors in these models. *Acta Crystallogr. A47*, 110−119.
(36) Xiang, D. F., Kolg, B., Fedorov, A. A., Meier, M. M., Fedorov, L. V., Nguyen, T. T., Sterner, R., Almo, S. C., Shoichet, B. K., and Raushel, F. M. (2009) Functional annotation and three-dimensional structure of Dr0930 from *Deinococcus radiodurans*, a close relative of phosphotriesterase in the amidohydrolase superfamily. *Biochemistry 48*, 2237−2247.
(37) Irwin, J. J., Raushel, F. M., and Shoichet, B. K. (2005) Virtual screening against metalloenzymes for inhibitors and substrates. *Biochemistry 44*, 12316−12328.
(38) Irwin, J. J., Shoichet, B. K., Mysinger, M. M., Huang, N., Colizzi, F., Wassam, P., and Cao, Y. (2009) Automated docking screens: A feasibility study. *J. Med. Chem. 52*, 5712−5720.
(39) Wlodek, S., Skillman, A. G., and Nicholls, A. (2010) Ligand entropy in gas-phase, upon salvation and protein complexation. Fast estimation with quasi-Newton Hessian. *J. Chem. Theory Comput. 6*, 2140−2152.
(40) Benning, M. M., Kuo, J. M., Raushel, F. M., and Holden, H. M. (1995) Three-dimensional structure of the binuclear center of phosphotriesterase. *Biochemistry 34*, 7973−7978.
(41) Ma, J. C., and Dougherty, D. A. (1997) The cation-π interaction. *Chem. Rev. 97*, 1303−1324.
(42) Liaw, S.-H., Chen, S.-J., Ko, T.-P., Hsu, C.-S., Chen, C.-J., Wang, A. H.-J., and Tsai, Y.-C. (2003) Crystal structure of D-aminoacylase from *Alcaligenes faecalis* DA1. *J. Biol. Chem. 278*, 4957−4962.
(43) Lai, W.-L., Chou, L.-Y., Ting, C.-Y., Kirby, R., Tsai, Y.-C., Wang, A. H.-J., and Liaw, S.-H. (2004) The functional role of the binuclear metal center in D-aminoacylase: One-metal activation and second-metal attenuation. *J. Biol. Chem. 279*, 13962−13967.
(44) Liu, J., Asano, Y., Ikoma, K., Yamashita, S., Hirose, Y., Shimoyama, T., Takahashi, S., Nakayama, T., and Nishino, T. (2012) Purification, characterization and primary structure of a novel N-acyl-D-amino acid amidohydrolase from *Microbacterium natoriense* TNJL143-2. *J. Biosci. Bioeng. 114*, 391−397.
(45) Ju, X., Yu, H.-L., Pan, J., Wei, D.-Z., and Xu, J.-H. (2010) Bioproduction of chiral mandelate by enantioselective deacylation of α-acetoxyphenylacetic acid using whole cells of newly isolated *Pseudomonas* sp. ECU1011. *Appl. Microbiol. Biotechnol. 86*, 83−91.